# Relationship between machinability index and in-process parameters during orthogonal cutting of steels☆

I. Arriola [a,b,*], E. Whitenton [c], J. Heigel [d], P.J. Arrazola (2)[a]

[a] Faculty of Engineering, Mondragon University, Mondragón, Spain
[b] marGUNE Center, Eibar, Spain
[c] National Institute of Standards and Technology[1], Gaithersburg MD, USA
[d] KT Consulting, Inc., Antioch CA, USA

ARTICLE INFO

*Keywords:*
Plastic strain
Temperature
Machinability index

ABSTRACT

Temperature and plastic strain maps were obtained during orthogonal cutting of two steels with different machinability indexes using a high speed dual spectrum (visible and infrared) and visible spectrum cameras, respectively. Surface and internal temperature were compared by simultaneous measurements with a thermal camera and thermocouples embedded in the flank face of the cutting tool. A cause effect relationship between the machinability index and the analyzed *in process* variables is determined. This will help with developing a practical tool for the scientific design of different machinability index materials, as well as an alternative method to time consuming and expensive standardized machinability tests.

## 1. Introduction

Machinability can be defined as the ability of a material to be machined using machine tools [1]. Furthermore, machinability can be tailored with modifications in the chemical composition to obtain a stable layer at the tool chip interface [2,3] that protects the tool [4] and leads to less tool wear. These improvements have been observed in post process research where cutting edge geometry [5], wear protection, thermal barrier [6], and friction are pointed as main factors affected by this stable layer.

Today industry is getting more interested in knowing before hand this machinability index, because machining performance will be affected with regard to the optimum economic level of machine utilization [1]. There are different ways to measure this index or determine the boundaries of machining process variables of the material to be processed, the so called 'process window'. Possible methods include cutting speed tests, radio active isotope wear tests, single or double tool temperature measurement, and cutting force measurement [1]. However, industry keeps conduct ing time consuming and costly standardized tests because there are as many tests as combinations of tool material and work material.

This research seeks a cause effect relationship between machinability rate and *in process* variables (cutting forces, temperature, and plastic strain) through experimental study. This is accomplished by, first, *in process* parameters measurement employing advanced experimental techniques such as a dual spectrum camera, embedded thermocouples, and a high speed camera. Second, the analysis is extended and complemented with detailed characterization (material flow stress, friction, thermal conductivity, and heat capacity) of the machined steels and tool deposition analysis. These experiments justify not only the effect of the machinability rate on machining performance, but also the effect exerted on many other possible lines of action simulta neously through short run tests. Therefore, an attempt is made to develop a practical tool for the scientific design of more machinable materials and to reduce the need for tedious, time consuming, and expensive machinability tests (ISO 3685).

## 2. Experimental design

This study is mainly focused on the understanding of the machinability difference between American Iron and Steel Institute (AISI) 4140 Standard (42CD4 E) and AISI 4140 MECA MAX® Plus (42CD4 Plus) with different V15 values (machinability index), $295 \pm 25$ m min$^{-1}$ and $400 \pm 25$ m min$^{-1}$ respectively (detailed steels property characterization [6,7]). Orthogonal cutting experiments were performed dry at the cutting speeds of 300 m min$^{-1}$ and 400 m min$^{-1}$ and uncut chip thickness of 0.1 mm, 0.2 mm, and 0.3 mm, with several repetitions to estimate the uncertainty. Commercially available uncoated TPG321 type tungsten carbide inserts with 0° rake angle, 5° clearance angle, and 5 μm cutting edge radius were used. This tool is subjected to electro discharge machining (EDM) to obtain a flat perpendicular surface to the optical axis of the dual bandwidth microscope and known

☆ *Disclaimer*: This document is an official contribution of the National Institute of Standards and Technology and is not subject to copyright in the United States. The National Institute of Standards and Technology does not recommend or endorse commercial equipment or materials, nor does it imply that the equipment or materials shown are necessarily the best available for the purpose.

* Corresponding author.

[1] This document is an official contribution of the National Institute of Standards and Technology and is not subject to copyright in the United States. The National Institute of Standards and Technology does not recommend or endorse commercial equipment or materials, nor does it imply that the equipment or materials shown are necessarily the best available for the purpose.

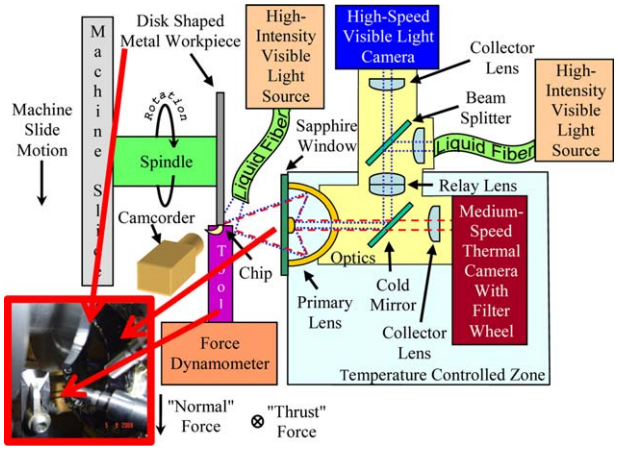


**Fig. 1.** Schematic diagram of the dual spectrum set up [9].

emissivity values [6]. The workpiece was a cylindrical disk with a diameter of approximately 80 mm and 3 mm of thickness.

### 2.1. Temperature measurement

Surface and internal temperatures were compared by simulta neous measurements with a thermal camera and thermocouples embedded in the flank face of the cutting tool in order to observe if thermal values were different or not in the center [8] and side [6] of the tool during orthogonal cutting tests under dry conditions.

#### 2.1.1. Infrared camera

Micro scale temperature maps were obtained using a custom built high speed dual spectrum system (see Fig. 1) at the National Institute of Standards and Technology (NIST). This is a simulta neous synchronized visible and thermal imaging system which is composed of a thermal infrared camera and a visible camera. The main lens is a 15× reflective lens that passes both visible and infrared light. The cold mirror reflects the visible light to the visible camera and transmits infrared light to the thermal camera.

The infrared camera was calibrated using a traceable calibrated blackbody that ranges from 350 °C to 1100 °C setting the camera at 19 μs of integration time. A cubic polynomial equation converts camera readings of the machining process to spectral (black body) radiance temperatures. Afterwards, the locations of the tool, chip, and workpiece were determined from visible images captured by the synchronized high speed camera. Using this information, the correct emissivity curve was applied to each region [6].

A data acquisition system records the timing of the thermal and visible spectrum images, along with analog data such as cutting forces. Thus, true temperature at any given location in the tool and corresponding cutting forces are played back in a synchronized manner.

Fig. 2 shows an example of (i) a standard camcorder image, (ii) the visible spectrum image captured at 30,000 frames per second

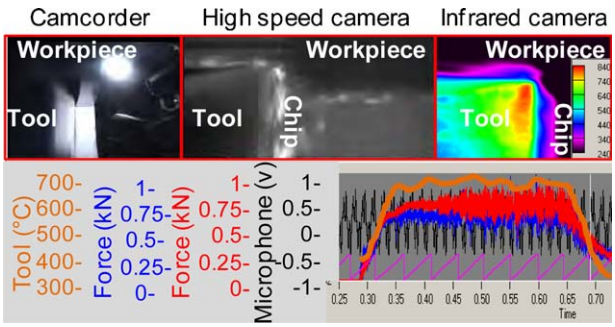


**Fig. 2.** Output parameters from dual spectrum equipment after orthogonal tests.

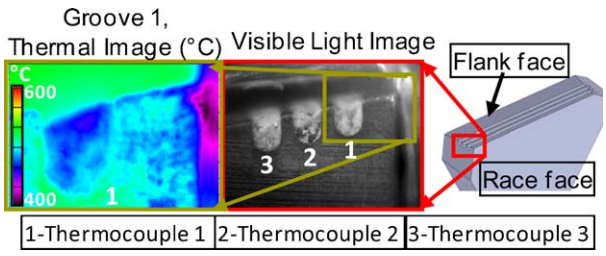


**Fig. 3.** Schematic diagram of the tool insert with embedded thermocouples (right) and visual (middle) and infrared (left) images of this tool during orthogonal cutting.

and 33 μs integration time, yielding 256 × 128 pixel size, and (iii) the spectral radiance maps acquired at 300 frames per second and 19 μs integration time, from 3.8 μm to 5.1 μm in wavelength with 160 × 120 pixel size.

#### 2.1.2. Embedded thermocouples

Simultaneous temperature measurements were run using both a thermal camera and thermocouples embedded within a custom modified cutting tool. The tool design contained three slots on the flank face precisely made by EDM for placing embedded thermocouples (Fig. 3). This gap is filled with high temperature cement which provides a consistent and precise fit between the thermocouple and the tool insert, as well as thermal conductivity and thermal expansion similar to that of the cutting tool. Three grounded metal sheath 0.25 mm diameter type K thermocouples were used.

The temperature sensitive portions of the thermocouples were positioned so that they were approximately where the center of the chips would be during machining and 0.5 mm (thermocouple 1), 1 mm (thermocouple 2) and 1.5 mm (thermo couple 3) far from the tool chip interface. In this way: (i) the gradients are much smaller in the perpendicular direction to the chip flow direction than from rake face to the bottom of the insert, so uncertainties are smaller [10] and (ii) slots are much easier to manufacture precisely and with repeatable locations for the thermocouples.

### 2.2. Chip formation analysis

Chip formation analysis with a visible high speed camera provided observations of the type of chip (chip thickness, serration phenomena, and shear angle) and plastic strain. The set up was composed of (i) the Photron Fastcam SA1.1, (ii) a 15× microscope objective, and (iii) four powerful white lights guided with fibre optics. As a result, 128 × 128 pixel and 128 × 64 pixel resolution images were captured at a frequency of 300,000 and 180,000 frames per second and 1.76 μs integration time, respectively (see Fig. 4).

Digital image correlation (DIC, Limess) [7] was employed to obtain plastic strain maps from high speed camera videos recorded during the orthogonal tests. This software matches small square subsets of an undeformed image to locations in an image of the surface after deformation to calculate plastic strain.

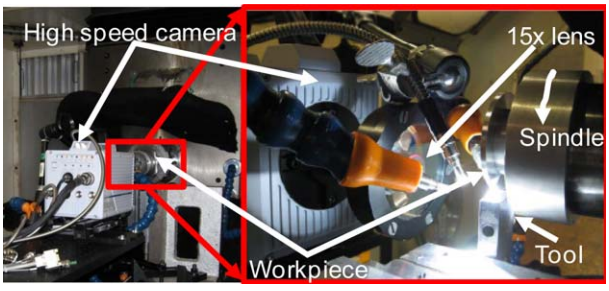


**Fig. 4.** Visual spectrum high speed camera set up during orthogonal cutting tests.

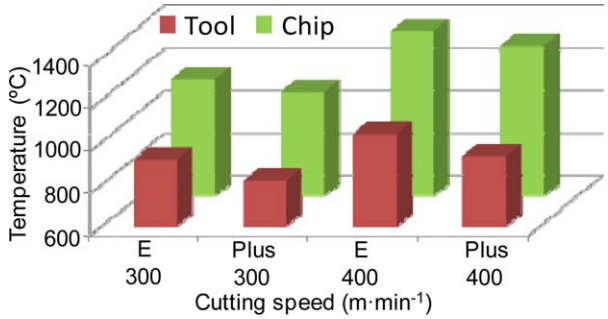


**Fig. 5.** Maximum tool and chip temperature at the cutting speeds of 300 and 400 m min$^{-1}$ and uncut chip thickness of 0.2 mm when machining 42CD4E and 42CD4Plus.

## 3. Results

Thermal infrared measurements show that the improved machinability steel does lead to reduced temperatures in the tool chip region (see Fig. 5). These reductions exceed the measurement uncertainties for temperatures on the chip and tool of ±40 °C and ±20 °C, respectively [6]. The greatest differences are observed at the higher cutting speed of 400 m min$^{-1}$, which is consistent with the precipitation and consequent deposition of the MnS layer on the rake face [2]. This also matches with the V15 of the 42CD4 Plus steel. The cutting as well as thrust forces are lower for AISI 4140 Plus under all conditions. For instance, at the cutting speed of 400 m min$^{-1}$ and uncut chip thickness of 0.2 mm, the cutting forces are similar but slightly lower (4 N difference), whereas feed forces are considerably lower (20 N difference) exceeding the measurement uncertainty of ±10 N.

The embedded thermocouple tools indicate changes in measured temperatures with increased cutting speed similar to the infrared camera. For instance, both show a difference of 30 °C between materials. Furthermore, Fig. 6 shows good agreement between infrared camera and embedded thermocouple tempera ture readings. These results indicate that a thermal camera measurement of the side of the cutting tool is representative of the temperature within the tool during steady state cutting. Concerning chip formation analysis, the results presented here should be considered as qualitative since the measurement uncertainty cannot currently be quantified.

There is no appreciable difference in the type of chip between both steels, except thinner (between 10 and 15%) chips for 42CD4 Plus. However, better machinability grade is correlated with slightly higher plastic strain when varying the cutting speed as well as uncut chip thickness. For instance, at the cutting speed of 400 m min$^{-1}$ and uncut chip thickness of 0.2 m, 42CD4E is subjected to 1.47 (see Fig. 7 top) plastic strain in the shear plane, whereas 42CD4 Plus rises to 1.51 (see Fig. 7 bottom). This

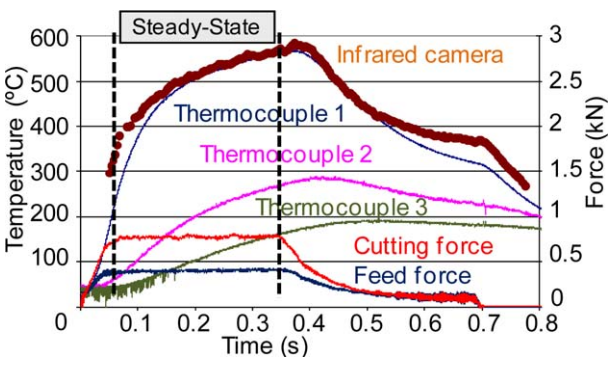


**Fig. 6.** Temperature profile recorded with infrared camera and embedded thermocouples. 42CDPlus at the cutting speed of 400 m min$^{-1}$ and uncut chip thickness of 0.1 mm.

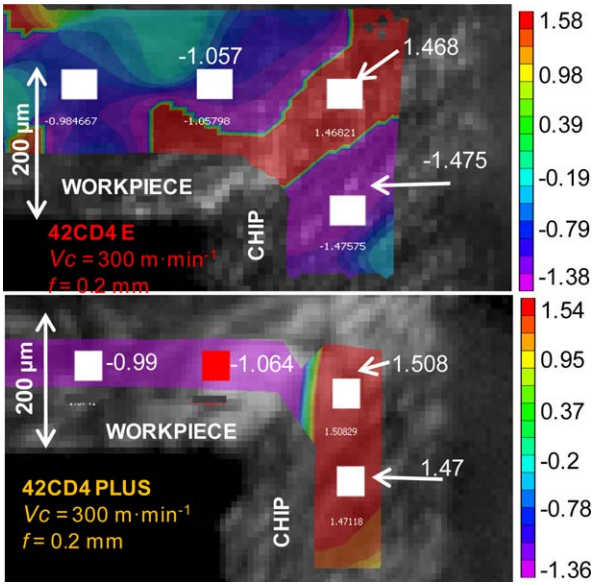


**Fig. 7.** Equivalent plastic strain map when cutting 42CD4 Plus and 42CD4 E at the cutting speed of 400 m min$^{-1}$ and uncut chip thickness of 0.2 mm.

can be understood because the decrease in temperature corresponds to an increase in the strain rate, as other authors [11] have reported. However, in some working conditions, e.g., at the cutting speed of 300 m min$^{-1}$ and 0.2 mm of uncut chip thickness, similar values are found. That is 1.47 of plastic strain is exerted on the shear plane when 42CD4E is machined whereas 42CD4 Plus reaches 1.48.

As it has not been possible to measure the plastic deformation on the secondary zone (due to lack of resolution and light) the maximum values measured are situated on the shear plane ranging from 1.38 to 1.5, which match closely with results found by Jaspers et al. [12] in all the conditions analyzed.

During the detailed material characterization, quasi static testing and dynamic tests are performed using a tensile test machine and the NIST Pulse Heated Split Hopkinson bar [13], respectively (see Fig. 8). Results show the strain hardening and thermal softening effects. In addition, 42CD4 Plus reaches 75 MPa and 190 MPa higher values of flow stress compared to 42CD4E at the highest strain rate and highest temperature tested, respec tively, and when plastic strain is between 0.1 and 0.2. These higher values of flow stress can be due to effective blockage of the movement of dislocations by nonmetallic oxides (Ca, Mn, Se, . . .) as observed by other authors [14], too.

The higher flow stresses of the improved machinability steel could lead to higher pressure on the rake face, which increases friction and cutting forces, resulting in higher temperatures. Therefore, the tool would be subjected to a faster wear since

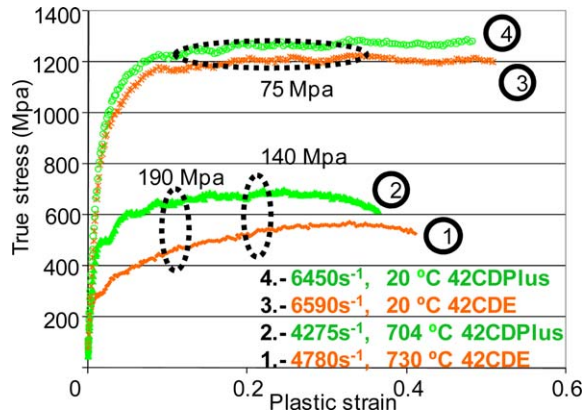


**Fig. 8.** Temperature effect (thermal softening) on flow stress of 42CD4E (orange) and 42CD4 Plus (green) at high strain rates.

temperature activates exponential wear mechanisms. Furthermore, the measured lower heat capacity ($C_p$) and thermal conductivity ($K$) of 42CD4 Plus ($C_p = 0.1349\ \ln(T) - 0.2673$ and $K = 0.0001\ T^2 + 0.0777\ T + 29$) compared to 42CD4E ($C_p = 0.1349\ \ln(T) - 0.1709$ and $K = 0.0001\ T^2 + 0.0715\ T + 36$) would lead to even higher machining temperatures [10].

Nevertheless, Albrecht [2,10] tests yield that the 42CD4 Plus friction value is lower than 42CD4E, 0.22 and 0.26 respectively. Experimental results show that best machinability grade steel is correlated with lower temperatures and feed forces.

The observed *in process* parameters value differences and material properties between different machinability index steels can be attributed to the different inclusion populations (Mn, S, Ca, and Se) of both steels in the chemical composition and found deposited on the rake face, as SEM analysis shows. These inclusions can become a deformable solid or gel liquid layer that improves chip tool workpiece interaction, obtaining better machining performance and thus better machinability index.

## 4. Conclusions

Side temperature measurements using the infrared technique confirm lower temperatures with better machinability grade steel. Additionally, similar surface and internal temperatures were determined by simultaneous measurements with a thermal camera and three thermocouples embedded in the flank face of the cutting tool. The embedded thermocouple method is cheaper and easier than the sophisticated infrared methodology.

Maximum values of plastic deformations were measured in the shear plane, with the best machinability grade steel having slightly higher plastic deformations.

The relationship between machinability index of the analyzed steels and *in process* parameters (feed forces, temperature, and plastic strain) measurement results was determined. Lower feed forces, lower friction value, lower temperatures, and higher plastic strain values correlate with better machinability index.

The measurements presented in this paper demonstrate progress towards a practical instrumented tool for the scientific design of more machinable materials by short run tests and a reduced need for long run (tedious, time consuming, and expensive) machinability tests (ISO 3685).

## Acknowledgments

The authors thank the Basque and Spanish Governments for the financial support given to the projects MANUFACTURING 0,0 II (code IE 09 254) and METINCOX (DPI2009 14286 C02 01 and PI2010 11). Authors also thank Sidenor (Spain), Ainhara Garay and Andoni Villar of MU (Spain) and April Cooke and Robert Ivester of NIST (USA) for support given to this work. For further information contact e mail: iarriola@tekniker.es.

## Disclaimer



## References

[1] Micheletti GG (1970) Work on Machinability in the Co-operative Group C of CIRP and Outside this Group. *Annals of CIRP* 18:13–30.
[2] Hamann JC, Guillot D, Le Maitre F (1996) Machinability Improvement of Steels at High Cutting Speeds-study of Tool/Work Material Interaction. *Annals of the CIRP* 45(1):87–92.
[3] M'Saoubi R, Chandrasekaran H (2005) Innovative Methods for the Investigation of Tool–Chip Adhesion and Layer Formation During Machining. *Annals of the CIRP* 54(1):59–62.
[4] Venkatesch VC (1993) A Study of Chip Surface Characteristics During Machining of Steels. *Annals of the CIRP* 42(1):631–636.
[5] Denkena B, Becker JC, de Leon-Garcia L (2005) Study of the Influence of the Cutting Edge Microgeometry on the Cutting Forces and Wear in Turning Operations. *8th Workshop on Modelling of Machining Operations*, 503–507.
[6] Arrazola PJ, Arriola I, Davies MA, Cooke AL, Dutterer BS (2008) The Effect of Machinability on Thermal Fields in Orthogonal Cutting of AISI 4140 Steel. *Annals of the CIRP* 57(1):65–68.
[7] Arriola I. (2010) *AISI 4140 Steel's Machinability Comprehension Analyzing In-process Parameters by Advance Measurement Techniques*, PhD Thesis.
[8] Narayanan V, Krishnamurthy K, Chandrasekar S, Farris TN, Madhavan V (2001) Measurement of the Temperature Field at the Tool–Chip Interface in Machining. *Proceedings of the ASME International Mechanical Engineering*, NY, 1–8.
[9] Whitenton E, Heigel J, Cooke A, Arriola I (2010) Recent Experiments Assessing the Uncertainty Of Metal Measurements When Using the NIST High-speed Cual-spectrum Optical System. *Thermosense Conference*, Florida, .
[10] Attia MH, Kops L (2004) A New Approach to Cutting Temperature Prediction Considering the Thermal Constriction Phenomenon in Multi-layer Coated Tools. *Annals of the CIRP* 53(1):47–52.
[11] Saldana C, Shankar MR, Murthy TG, Huang C, Gnanamanickam E, Chandrasekar S (2008) Zener–Hollomon Parameter and Microstructure Prediction in Machining. *11th CIRP Conf. Mod.*, 129–137.
[12] Jaspers SPFC, Dautzenberg JH (2002) Material Behavior in Metal Cutting: Strains, Strain Rates and Temperatures in Chip Formation. *Journal of Materials Processing Technology* 121:123–135.
[13] Burns TJ, Mates SP, Rhorer RL, Whitenton EP, Basak D (2007) Recent Results from the NIST Pulse-Heated Kolsky Bar. *Proceedings of the 2007 Society for Experimental Mechanics*, June 3–6, .
[14] Nurul Amin AKM, Kurchenko AI, Talantov NP (1984) Investigation of the Physical Causes of Improved Machinability of Steel Alloyed with Calcium. *Mechanical Engineering Research Bulletin (Dhaka)* 1:9–16.